Quantum Chemical Characterization of Methane Metathesis in L_2MCH_3 (L = H, Cl, Cp, Cp*; M = Sc, Y, Lu)

Edward C. Sherer and Christopher J. Cramer*

Department of Chemistry and Supercomputer Institute, University of Minnesota, 207 Pleasant Street SE, Minneapolis, Minnesota 55455-0431

Received November 22, 2002

The dimerization, unimolecular methane ejection, and bimolecular methane metathesis reactions of L_2MCH_3 species where L = H, Cl, Cp, and Cp* and M = Sc, Y, and Lu are modeled at the density functional level (B3LYP) using a relativistic effective core potential basis set. Results for cases with H or Cl ligands are in poor quantitative agreement with analogous results for cases with Cp* ligands; in some instances, Cp ligands provide results in good agreement with those for Cp*, but in the case of methane metathesis, activation enthalpies are underestimated by 3−4 kcal mol^{-1} with the unmethylated ligand. Unimolecular methane ejection via formation of a tuck-in complex versus bimolecular methane metathesis is predicted potentially to be a competitive process for Sc, but to be comparatively too high in energy for Y and Lu to be thermodynamically significant under typical sets of reaction conditions. The difference is ascribable to the shorter metal−ligand distances observed for Sc. For $(Cp^*)_2LuCH_3$, quantum mechanical tunneling is predicted to increase the overall rate of methane metathesis by factors of 4−93 over the temperature range 300−400 K. When tunneling is accounted for in the experimentally measured rate constants, a semiclassical enthalpy of activation of 19.2 kcal mol^{-1} is predicted for the methane metathesis reaction, in good agreement with a direct prediction from density functional theory of 20.3 kcal mol^{-1}.

Introduction

Organometallic species find use as catalysts in many economically important synthetic processes. One subset, metallocenes, has shown particular utility as catalysts for olefin polymerization and further evince considerable potential to activate alicyclic and aliphatic C−H bonds.[1−11] Watson and co-workers have studied in some detail C−H bond activation by lutetiocenes,[2,3,12−17] the diverse chemistry of which reaction has also been the subject of other experimental and theoretical attention.[18−26] On the basis of key similarities and differences in reactivity, the related chemistries of organometallic analogues containing scandium and yttrium have attracted considerable interest too.[20,21,25−34]

One particularly interesting group of reactions in this general category is detailed in Scheme 1. Using ^{13}C-

(1) Wailes, P. C.; Coutts, R. S. P.; Weigold, H. *Organometallic Chemistry of Titanium, Zirconium, and Hafnium*; Academic: New York, 1974.
(2) Watson, P. L.; Parshall, G. W. *Acc. Chem. Res.* **1985**, *18*, 51.
(3) Davies, J. A.; Watson, P. L.; Liebman, J. F.; Greenberg, A. *Selective Hydrocarbon Activation: Principles and Progress*; VCH Publishers: New York, 1990.
(4) Hall, C.; Perutz, R. N. *Chem. Rev.* **1996**, *96*, 3125.
(5) Ephritikhine, M. *Chem. Rev.* **1997**, *97*, 2193.
(6) Kaminsky, W.; Arndt, M. *Adv. Polym. Sci.* **1997**, *127*, 143.
(7) Shilov, A. E.; Shul'pin, G. B. *Chem. Rev.* **1997**, *97*, 2879.
(8) Das, P. K.; Dockter, D. W.; Fahey, D. R.; Lauffer, D. E.; Hawkins, G. D.; Li, J.; Zhu, T.; Cramer, C. J.; Truhlar, D. G.; Dapprich, S.; Froese, R. D. J.; Holthausen, M. C.; Liu, Z.; Mogi, K.; Vyboishchikov, S.; Musaev, D. G.; Morokuma, K. In *Transition State Modeling for Catalysis*; Truhlar, D. G., Morokuma, K., Eds.; ACS Symposium Series 721; American Chemical Society: Washington, DC, 1999; p 208.
(9) Dedieu, A. *Chem. Rev.* **2000**, *100*, 543.
(10) Ustynyuk, Y. A.; Ustynyuk, L. Y.; Laikov, D. N.; Lunin, V. V. *J. Organmet. Chem.* **2000**, *597*, 182.
(11) Crabtree, R. H. *J. Chem. Soc., Dalton Trans.* **2001**, 2437.
(12) Watson, P. L.; Roe, D. C. *J. Am. Chem. Soc.* **1982**, *104*, 6471.
(13) Watson, P. L. *J. Am. Chem. Soc.* **1983**, *105*, 6491.
(14) Watson, P. L. *J. Chem. Soc., Chem. Commun.* **1983**, 276.
(15) Watson, P. L. In *Selective Hydrocarbon Activation: Principles and Progress*; Davies, J. A., Watson, P. L., Greenberg, A., Liebman, J. F., Eds.; VCH: New York, 1990; p 79.
(16) Jahns, V.; Kostlmeier, S.; Kotzian, M.; Rosch, N.; Watson, P. L. *Int. J. Quantum Chem.* **1992**, *44*.
(17) Watson, P. L.; Calabrese, J. C. Unpublished results cited in ref 3.
(18) Schumann, H.; Genthe, W.; Bruncks, N.; Pickardt, J. *Organometallics* **1982**, *1*, 1194.
(19) Gong, L.; Streitweiser, A.; Zalkin, A. *J. Chem. Soc., Chem. Commun.* **1987**, 460.
(20) Evans, W.; Foster, S. E. *J. Organomet. Chem.* **1992**, *433*, 79.
(21) Haar, C. M.; Stern, C. L.; Marks, T. J. *Organometallics* **1996**, *15*, 1765.
(22) Scherer, W.; Runte, O.; Herrmann, W. A. *Inorg. Chem.* **1997**, *36*, 3545.
(23) Schumann, H.; Keitsch, M. R.; Winterfeld, J.; Muhle, S.; Molander, G. A. *J. Organomet. Chem.* **1998**, *559*, 181.
(24) Schumann, H.; Keitsch, M. R.; Winterfeld, J.; Muhle, S.; Molander, G. A. *J. Organomet. Chem.* **1998**, *559*, 181.
(25) Schumann, H.; Rosenthal, E. C. E.; Demtschuk, J. *Organometallics* **1998**, *17*, 5324.
(26) Eppinger, J.; Spiegler, M.; Heringer, W.; Herrmann, W. A.; Anwander, R. *J. Am. Chem. Soc.* **2000**, *122*, 3080.
(27) Schumann, H.; Erbstein, F.; Karasiak, D. F.; Fedushkin, I. L.; Demtschuk, J.; Girgsdies, F. *Z. Anorg. Allg. Chem.* **1999**, *625*, 781.
(28) Schumann, H.; Lee, P. R.; Dietrich, A. *Chem. Ber.* **1990**, *123*, 1331.
(29) Deelman, B.-J.; Teuben, J. H.; Macgregor, S. A.; Eisenstein, O. *New J. Chem.* **1995**, *19*, 691.
(30) Fryzuk, M. D.; Giesbrecht, G.; Rettig, S. J. *Organometallics* **1996**, *15*, 3329.
(31) Hagadorn, J. R.; Arnold, J. *Organometallics* **1996**, *15*, 984.
(32) Casey, C. P.; Hallenbeck, S. L.; Wright, J. M.; Landis, C. R. *J. Am. Chem. Soc.* **1997**, *119*, 9680.
(33) Putzer, M. A. *Z. Anorg. Allg. Chem.* **1999**, *625*, 1777.
(34) Nagayama, S.; Kobayashi, S. *Angew. Chem., Int. Ed.* **2000**, *39*, 567.

10.1021/om0209632 CCC: $25.00
Publication on Web 03/20/2003

Scheme 1

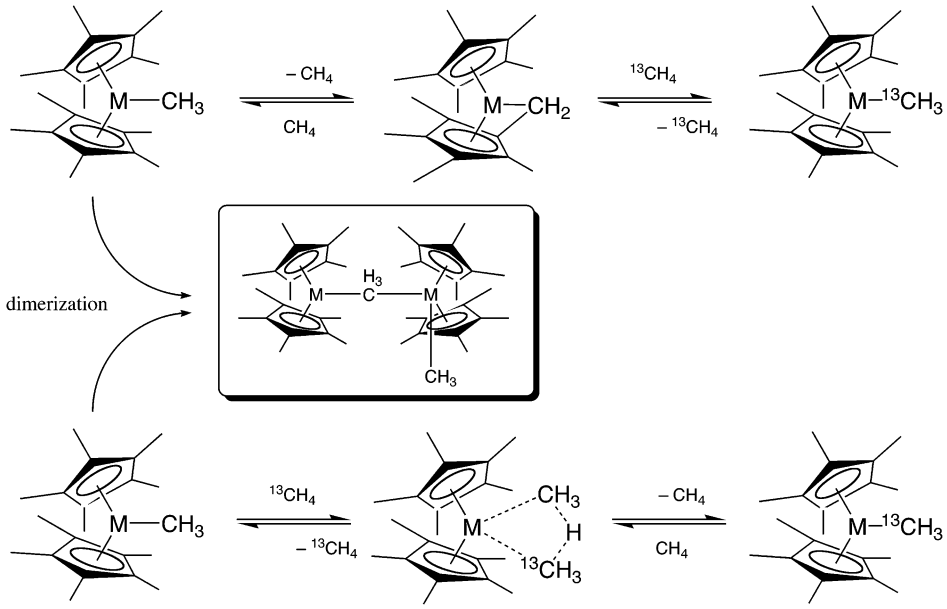

labeled methane, Watson and co-workers[2,3,13–15] have demonstrated that permethyl(methyllutetiocene), which exists as an equilibrium mixture of monomers and dimers at typical experimental temperatures, catalyzes the C–H bond activation of methane. On the basis of various factors, they infer the lower route in Scheme 1 to be the only important one for methane metathesis, although there is precedent for the upper path based on known structures for metallocenes incorporating metals *other* than lutetium, e.g., scandium.[35]

Bolstered most recently by the generally good accuracy of density functional theory (DFT) calculations for organometallic species,[36–42] molecular modeling has played an important role in mapping out microscopic reaction coordinates for organometal-catalyzed transformations. The identification of all reactive intermediates and transition state (TS) structures on a putative reaction coordinate can be particularly valuable when the specifics of the reaction may render difficult the experimental detection or inference of these species. In addition, theoretical work permits the systematic variation of various aspects of the model (e.g., ligands) over a broad range to assess the sensitivity of the reaction to those variables. As such, C–H bond activation and other bond-insertion reactivities have been the subject of extensive theoretical study.[10,16,29,32,43–54]

In this work, we examine metallocenes and smaller model systems incorporating Sc, Y, and Lu with the goal of better understanding their structure and reactivity in serving as catalysts for C–H bond activation, in particular with respect to methane/methane metathesis. Using density functional theory, we characterize relevant reaction coordinates for this process varying the ligands on the metal through H, Cl, η^5-cyclopentadienide (Cp), and η^5-permethylcyclopentadienide (Cp*). We note that, historically, H and Cl have been employed as economical alternatives to Cp and Cp* groups in molecular calculations, but their ability to serve as electronic/steric surrogates for these larger groups is by no means established.

Computational Methods

All structures were fully optimized at the density functional level of theory. For geometry optimizations, we employed the hybrid B3LYP functional,[55,56] which combines Becke's nonlocal exchange functional[57] with the nonlocal correlation functional of Lee, Yang, and Parr.[58] The compact effective core potential basis of Stevens et al. (CEP-31G)[59] incorporating scalar relativistic effects was used for Cl, Sc, Y, and Lu and the 6-31G(d,p) basis set[60] for H and C; we will refer to this combination as ECP1 below.

(35) Thompson, M. E.; Baxter, S. M.; Bulls, A. R.; Burger, B. J.; Nolan, M. C.; Santasiero, B. D.; Schaefer, W. P.; Bercaw, J. E. *J. Am. Chem. Soc.* **1987**, *109*, 203.
(36) Frenking, G.; Antes, I.; Böhme, M.; Dapprich, S.; Ehlers, A. W.; Jonas, V.; Neuhaus, A.; Otto, M.; Stegmann, R.; Veldkamp, A.; Vyboishchikov, S. F. In *Reviews in Computational Chemistry*; Lipkowitz, K. B., Boyd, D. B., Eds.; VCH: New York, 1996; Vol. 8, p 63.
(37) *Chemical Applications of Density Functional Theory*; Laird, B. B., Ross, R. B., Ziegler, T., Eds.; ACS Symposium Series 629; American Chemical Society: Washington, DC, 1996.
(38) Fey, N. *J. Chem. Technol. Biotechnol.* **1999**, *74*, 852.
(39) Koch, W.; Holthausen, M. C. *A Chemist's Guide to Density Functional Theory*; Wiley-VCH: Weinheim, 2000.
(40) Urnezius, E.; Brennessel, W. W.; Cramer, C. J.; Ellis, J. E.; Schleyer, P. v. R. *Science* **2002**, *295*, 832.
(41) Frunzke, J.; Lein, M.; Frenking, G. *Organometallics* **2002**, *21*, 3351.
(42) Cramer, C. J. *Essentials of Computational Chemistry: Theories and Models*; Wiley: Chichester, 2002.
(43) Rabaa, H.; Saillard, J.-Y.; Hoffmann, R. *J. Am. Chem. Soc.* **1986**, *108*, 4327.
(44) Folga, E.; Ziegler, T.; Fan, L. *New J. Chem.* **1991**, *15*, 741.
(45) Folga, E.; Ziegler, T. *Can. J. Chem.* **1992**, *70*, 333.
(46) Rappe, A. K.; Upton, T. H. *J. Am. Chem. Soc.* **1992**, *114*, 7507.
(47) Ziegler, T.; Folga, E.; Berces, A. *J. Am. Chem. Soc.* **1993**, *115*, 636.
(48) Ziegler, T.; Folga, E. *J. Organomet. Chem.* **1994**, *478*, 57.
(49) Adamo, C.; Barone, V. *J. Comput. Chem.* **2000**, *21*, 1153.
(50) Maron, L.; Eisenstein, O. *J. Phys. Chem.* **2000**, *104*, 7140.
(51) Maron, L.; Eisenstein, O. *J. Am. Chem. Soc.* **2001**, *123*, 1036.
(52) Maron, L.; Eisenstein, O.; Alary, F.; Poteau, R. *J. Phys. Chem.* **2002**, *106*, 1797.
(53) Maron, L.; Perrin, L.; Eisenstein, O. *J. Chem. Soc., Dalton Trans.* **2002**, 534.
(54) Perrin, L.; Maron, L.; Eisenstein, O. *Inorg. Chem.* **2002**, *41*, 4355.
(55) Becke, A. D. *J. Chem. Phys.* **1993**, *98*, 5648.
(56) Stephens, P. J.; Devlin, F. J.; Chabalowski, C. F.; Frisch, M. J. *J. Phys. Chem.* **1994**, *98*, 11623.
(57) Becke, A. D. *Phys. Rev. A* **1988**, *38*, 3098.
(58) Lee, C.; Yang, W.; Parr, R. G. *Phys. Rev. B* **1988**, *37*, 785.
(59) Stevens, W. J.; Krauss, M.; Basch, H.; Jasien, P. G. *Can. J. Chem.* **1992**, *70*, 612.
(60) Hehre, W. J.; Radom, L.; Schleyer, P. v. R.; Pople, J. A. *Ab Initio Molecular Orbital Theory;* Wiley: New York, 1986.

Although the B3LYP functional has been demonstrated to provide excellent molecular geometries in organometallic systems,[36,42,61] to include in particular lanthanides,[49] in our experience it can be somewhat less robust in the prediction of relative molecular energies along a reaction coordinate. To assess molecular energies in more detail, we have in some instances carried out single-point calculations using the exchange and correlation functionals of Perdew and coworkers[62,63] as modified by Adamo and Barone (*m*PWPW91).[64] In addition to calculations with the ECP1 basis set, we also carried out these calculations with diffuse functions added to the C atoms (6-31+G(d,p))[60]; we will refer to this basis set combined with CEP-31G for the other atoms as ECP2.

Analytic frequency calculations at the B3LYP/ECP1 level were carried out to verify the nature of all stationary points as either minima or transition-state (TS) structures. The frequencies were also used to compute 298 K thermal contributions to the enthalpy using the standard rigid-rotor-harmonic-oscillator approximation.[42] Because structures incorporating Cp* typically had many very small vibrational frequencies (below 20 cm^{-1}), we avoid discussion of molecular free energies, since absolute entropies predicted by the rigid-rotor-harmonic-oscillator approximation tend to be unreliable in such instances.

The reaction coordinate for methane metathesis shows substantial hydrogenic motion in its TS structures, so one may expect the reaction rate to include a substantial contribution from light-atom tunneling, even at typical experimental reaction temperatures on the order of 350 K; that is, the observed rate constant k_{obs} may be considered to be[42,65]

$$k_{obs} = \kappa(T) k_{class} \tag{1}$$

where κ is the temperature-dependent quantum mechanical transmission coefficient and k_{class} is the rate constant that would be observed in the absence of quantum effects.

Davies et al.[3] reported experimental activation enthalpies and entropies derived from the transition-state theory relationship[42,65,66]

$$\ln\left(\frac{k_{obs}}{T}\right) = \left(-\frac{\Delta H^{\ddagger}}{R}\right)\left(\frac{1}{T}\right) + \left(\frac{\Delta S^{\ddagger}}{R}\right) + \ln\left(\frac{k_B}{h}\right) \tag{2}$$

Thus, a plot of $\ln(k_{obs}/T)$ vs $1/T$ provides a best-fit line having slope $-\Delta H^{\ddagger}/R$ where R is the universal gas constant and the intercept permits determination of $\Delta S^{\ddagger}$. From their reported activation parameters, we have used eq 2 to compute k_{obs} values.

Note, however, that the use of eq 2 to determine thermodynamic activation parameters is justified only with *classical* rate constants. When rate constants from reactions whose rates include substantial contributions from tunneling are used in eq 2, derived activation enthalpies and entropies tend to values considerably smaller than those determined from the statistical mechanical partition functions of the relevant transition-state structures. In such instances, the comparison of experimental and computed thermodynamic activation parameters is not particularly meaningful, since the latter are indeed derived from computed molecular partition functions.

We can, however, compute classical rate constants k_{class} at a given temperature as k_{obs} divided by $\kappa(T)$ (cf. eq 1). A subsequent plot of $\ln(k_{class}/T)$ versus $1/T$ then provides a best-fit line having slope $-\Delta H^{\ddagger}/R$ where the new, classical $\Delta H^{\ddagger}$ may be compared directly to the value derived from computation.

To estimate κ, we have employed the truncated parabola method of Skodje and Truhlar.[42,67] In this approximation, the transmission coefficient associated with quantum effects on the reaction coordinate, κ, is computed as

$$\kappa(T) = \begin{bmatrix} \dfrac{\beta}{\beta - \alpha}\{e^{[(\beta-\alpha)(\Delta V^{\ddagger}-V)]} - 1\}, & \alpha \le \beta \\ \dfrac{\beta\pi/\alpha}{\sin(\beta\pi/\alpha)} - \dfrac{\beta}{\alpha - \beta} e^{[(\beta-\alpha)(\Delta V^{\ddagger}-V)]}, & \alpha \ge \beta \end{bmatrix} \tag{3}$$

where

$$\alpha = \frac{2\pi}{h\,\mathrm{Im}(\nu^{\ddagger})} \tag{4}$$

$$\beta = \frac{1}{k_B T} \tag{5}$$

T is temperature, $\Delta V^{\ddagger}$ is the zero-point-including activation barrier, V is the zero-point-including potential-energy difference between reactants and products (zero in the case of the symmetric metathesis reaction), $\mathrm{Im}(\nu^{\ddagger})$ is the magnitude of the imaginary vibration, h is Planck's constant, and k_B is Boltzmann's constant.

All calculations made use of the Gaussian98 electronic structure program suite.[68]

Results and Discussion

Nomenclature. We will refer to L_2MCH_3, its bi- and unimolecular methane displacement TS structures, and its dimer as **1**, **2**, **3**, and **4**, respectively. When only the cardinal is specified, the reference is generic. If a particular ligand and/or metal is implied, the cardinal will be modified with a suffix; for example, **1**-Lu refers to L_2MCH_3 with lutetium as the only metal atom under discussion but still any generic ligand, while **4**-Cp,Sc refers specifically to $[(Cp)_2ScCH_3]_2$.

Metallocene Structure. Selected geometrical parameters for **1**−**3**, respectively, are collected in Tables 1−3 (see Scheme 1 for reactions). The optimized structures for **1**-, **2**-, and **3**-Cp*,Lu are shown in Figure 1 as ball-and-stick models. Figure 2 provides a line drawing of the unimolecular TS structure for this case to facilitate data presentation in Table 2. Figure 3 provides a ball-and-stick depiction of the dimer **4**-Cp,Lu, also labeled to facilitate data presentation in Table 4, where selected geometrical data are collected for all of the metallocene dimers **4**.

(61) Siegbahn, P. E. M.; Blomberg, M. R. A. *Chem. Rev.* **2000**, *100*, 421.
(62) Perdew, J. P.; Burke, K.; Wang, Y. *Phys. Rev. B* **1996**, *54*, 16533.
(63) Burke, K.; Perdew, J. P.; Wang, Y. In *Electronic Density Functional Theory. Recent Progress and New Directions*; Dobson, J. F., Vignale, G., Das, M. P., Eds.; Plenum Press: New York, 1998; p 81.
(64) Adamo, C.; Barone, V. *J. Chem. Phys.* **1998**, *108*, 664.
(65) Steinfeld, J. I.; Francisco, J. S.; Hase, W. L. *Chemical Kinetics and Dynamics*, 2nd ed.; Prentice Hall: New York, 1999.
(66) Espenson, J. H. *Chemical Kinetics and Reaction Mechanisms*, 2nd ed.; McGraw-Hill: New York, 1995; p 200.
(67) Skodje, R. T.; Truhlar, D. G. *J. Phys. Chem.* **1981**, *85*, 624.
(68) Frisch, M. J.; Trucks, G. W.; Schlegel, H. B.; Scuseria, G. E.; Robb, M. A.; Cheeseman, J. R.; Zakrzewski, V. G.; Montgomery, J. A.; Stratmann, R. E.; Burant, J. C.; Dapprich, S.; Millam, J. M.; Daniels, A. D.; Kudin, K. N.; Strain, M. C.; Farkas, O.; Tomasi, J.; Barone, V.; Cossi, M.; Cammi, R.; Mennucci, B.; Pomelli, C.; Adamo, C.; Clifford, S.; Ochterski, J.; Petersson, G. A.; Ayala, P. Y.; Cui, Q.; Morokuma, K.; Salvador, P.; Dannenberg, J. J.; Malick, D. K.; Rabuck, A. D.; Raghavachari, K.; Foresman, J. B.; Cioslowski, J.; Ortiz, J. V.; Baboul, A. G.; Stefanov, B. B.; Liu, G.; Liashenko, A.; Piskorz, P.; Komaromi, I.; Gomperts, R.; Martin, R. L.; Fox, D. J.; Keith, T.; Al-Laham, M. A.; Peng, C. Y.; Nanayakkara, A.; Challacombe, M.; Gill, P. M. W.; Johnson, B.; Chen, W.; Wong, M. W.; Andres, J. L.; Gonzalez, C.; Head-Gordon, M.; Replogle, E. S.; Pople, J. A. *Gaussian 98 (Revision A.10)*; Gaussian, Inc.: Pittsburgh, PA, 2001.

Table 1. Selected Bond Distances (Å) and Bond Angles (deg) in 1 at the B3LYP/ECP1 Level[a]

L	M	*r*MC[b]	*r*MΩ[b]	∠ΩMΩ
H	Sc	2.161	1.833	120.5
	Y	2.328	1.997	115.6
	Lu	2.331	1.979	118.6
Cl	Sc	2.148	2.319	129.3
	Y	2.324	2.491	128.3
	Lu	2.312	2.468	129.5
Cp	Sc[c]	2.232	2.202	138.0
		(2.23)	(2.17)	(139.)
	Y	2.392	2.392	137.5
	Lu	2.363	2.363	135.7
Cp*	Sc[d]	2.251	2.226	143.6
		(2.243)	(2.171)	(144.6)
	Y	2.408	2.399	136.8
	Lu	2.375	2.373	142.2

[a] Structure **1** has formula R_2MCH_3; in columns, C refers to the methyl carbon and Ω refers either to a monatomic substituent H or Cl or to the centroid of a Cp or Cp* ring. [b] Average of two distances. [c] Values in parentheses are from a BP86 calculation with a polarized mixed double- and triple-ζ basis set; see ref 47. [d] Values in parentheses are from a single-crystal X-ray structure; see ref 35.

Table 2. Selected Bond Distances (Å) and Bond Angles (deg) in 2 at the B3LYP/ECP1 Level[a]

L	M	*r*MC	*r*MΩ	*r*MH	*r*CH	∠CMC	∠ΩMΩ
H	Sc	2.264	1.837	1.883	1.451	79.3	118.3
	Y	2.447	2.007	2.047	1.458	73.0	118.6
	Lu	2.439	1.975	2.033	1.464	73.7	117.0
Cl	Sc	2.266	2.331	1.873	1.448	79.0	122.5
	Y	2.439	2.498	2.037	1.457	73.2	124.0
	Lu	2.406	2.469	2.008	1.467	74.9	122.6
Cp	Sc	2.408	2.211	1.900	1.436	73.2	135.5
	Y	2.554	2.389	2.063	1.450	69.1	135.8
	Lu	2.522	2.356	2.036	1.453	70.4	134.2
Cp*	Sc	2.418	2.263	1.907	1.432	72.6	140.9
	Y	2.561	2.415	2.068	1.446	68.7	140.8
	Lu	2.525	2.383	2.033	1.450	70.1	141.1

[a] Structure **2** has formula $L_2M(CH_3)_2H$; in columns, C refers to the symmetrically related methyl carbons, Ω refers either to a monatomic substituent H or Cl or to the centroid of a Cp or Cp* ring, and H refers to the hydrogen atom in flight between the two methyl groups.

Structures **1** are routine: Ligand−metal bond lengths are shorter for **1**-Sc than for **1**-Y, as expected for a third-row/fourth-row progression; ligand−metal bond lengths for **1**-Lu are slightly shorter than for **1**-Y, also as one would expect from a combination of the lanthanide contraction and relativistic effects. Metal−methyl bond lengths in all three cases are longest when the other two ligands are Cp* groups, consistent with these groups being both the strongest electron donors and also the most sterically demanding. The steric influence of the Cp* methyl groups may be assessed from the change in the ΩMΩ angle (where Ω is a ring centroid in this case) on going from Cp to Cp*. In **1**-Y, where the metal−centroid distance is longest, this angle is the same to within 1 deg for Cp versus Cp*, but in **1**-Sc and **1**-Lu, with their somewhat shorter metal−centroid distances, the angle increases by about 6 deg upon methylation of the Cp rings. In the case of **1**-Cp*,Sc the theoretical level may be compared to a single-crystal X-ray structure,[35] and the agreement between the two is quite good (Table 1), providing some validation of the B3LYP/ECP1 level of theory applied to these specific systems. A separate comparison that is of some technical interest may be made for **1**-Cp,Sc, for which Ziegler et al.[47] have reported an optimized structure from the BP86 functional with a polarized mixed double- and triple-ζ basis set. The data in Table 1 show this structure to agree very closely with that from the B3LYP/ECP1 level, again supporting the notion that the efficient latter level of theory has excellent utility.

TS structures **2** also illustrate the different electronic and steric characteristics of Cp and Cp* compared to H and Cl ligands (Table 2). Relative to **1**, the two identical metal−methyl M−C bond lengths increase by about 0.1 Å for ligands H and Cl and by about 0.15 Å for Cp and Cp* (Table 2). Other metal−ligand distances are effectively unchanged in **2** compared to **1**. Interestingly, the distance between the metal and the hydrogen atom in flight between the two methyl groups is in every case about the same as the M−H distance in the reactants **1**-H (i.e., the metal to formal *ligand* H distance), and indeed this distance is substantially shorter in every case than the metal−methyl distance. Thus, there is clearly a strong metal−hydrogen interaction stabilizing the TS structure. The top-down view of **2**-Lu in Figure 1 makes this interaction clear. This additional metal−ligand interaction causes a reduction of about 1−7 deg in the ΩMΩ angle in nearly every case. In the case of Cp*, this reduction is small, presumably because of the greater steric demands of this ligand. Other than the ΩMΩ angle, the structural differences between structures **2**-Cp and **2**-Cp* are surprisingly small.

Structures **3** are TS structures leading to methane ejection and the formation of a "tuck-in" complex where one Cp* methyl group has become a methylene group coordinated to the metal (or, alternatively, one may view the Cp* ligand as having been converted to a tetramethylfulvene). Comparing TS structures **3** to **2**, the reacting Cp* ring is drawn closer to the metal by about 0.1 Å in **3**, the departing methane carbon is about the same distance from the metal, the H atom in flight is about 0.04 Å further from the metal, and all other geometric parameters are fairly similar except that the ΩMΩ angle is about 4 deg larger in **3** than in corresponding structures **2** (Table 3). To examine the importance of the other methyl groups on the Cp* ligand, a lutetiocene TS structure having only a single (reacting) methyl group on the ligand rings was also determined. As can be seen in Table 3, it has structural characteristics very similar to those for **3**-Cp*,Lu.

Finally, the dimer structures in Table 4 show overall trends similar to those for **1** with respect to critical bond lengths and angles. Owing to practical limitations, dimers **4** were computed only with L = Cp. However, a comparison between **4**-Cp,Lu and a single-crystal X-ray structure[2,17] of $[(Cp^*)_2LuCH_3]_2$ shows remarkably good agreement between the two (Table 4), suggesting that there are only minor structural consequences associated with ring methylation.

Bimolecular Methane Exchange. Prior work on hydrogen and methane activation by transition metals,[43,45−48] including lanthanides,[44,51−53] has typically involved replacement of computationally challenging Cp* groups by H or Cl in theoretical models, although more recent work has begun to include unmethylated Cp rings.[10,54] One feature we have observed with H and Cl ligands, which has also been reported previously, is the presence of **1**-methane complexes having significantly lower energy than separated reactants, where the

Table 3. Selected Bond Distances (Å) and Bond Angles (deg) in 3 at the B3LYP/ECP1 Level[a]

L	M	*r*MΩ1	*r*MΩ2	*r*MC1	*r*MC2	*r*MH	*r*C1H	*r*C2H	∠C1MC2	∠Ω1MΩ2
Cp*	Sc	2.222	2.173	2.397	2.475	1.942	1.468	1.483	72.9	144.3
	Y	2.398	2.331	2.553	2.626	2.104	1.468	1.503	69.0	144.7
	Lu	2.359	2.291	2.520	2.591	2.067	1.452	1.531	70.2	144.7
Cp[b]	Lu	2.346	2.271	2.519	2.587	2.062	1.451	1.532	70.3	141.7

[a] See Figure 2 for atom labeling in structure **3**; Ω refers to the centroid of a Cp, CpMe, or Cp* ring. [b] The Cp rings in this case are undecorated with methyl groups except for the one that is required for the reaction.

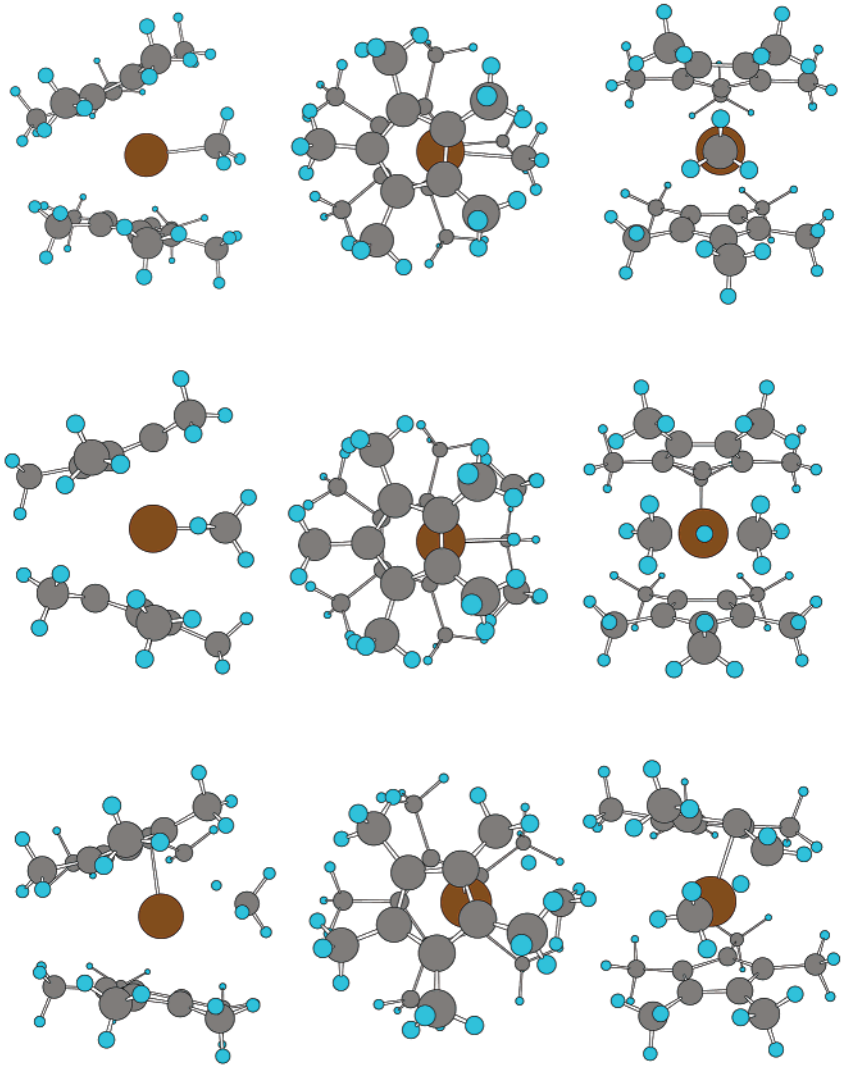

Figure 1. Optimized structures (B3LYP/ECP1) shown side-on (left), from above (center), and down the metal-reactive-center axis (right) for $(Cp^*)_2LuCH_3$ (top), the bimolecular methane metathesis TS structure (center), and the TS structure for internal displacement of methane (bottom). The central metal atom is brown, carbon atoms are gray, and hydrogen atoms are blue.

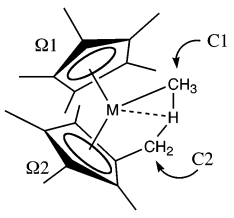

Figure 2. Internal methane displacement TS structure **3**; labeling for use in Table 2.

methane−metal interaction is through a metal-to-methane-hydrogen agostic interaction. With Cp and Cp*, however, we do not find such a complex on the bimolecular methane exchange reaction coordinate (there is only a very loose, very weak van der Waals complex on the potential energy surface that is predicted not to be bound when thermal contributions to the enthalpy are accounted for). Since these agostic complexes are not relevant with the larger Cp ligands, we will not discuss them further.

With respect to the energetics of methane metathesis via the bimolecular exchange pathway, Table 5 provides energies and 298 K enthalpies of activation computed for this process for all combinations of metal and ligand. Thermal contributions to the enthalpy of activation are not particularly sensitive to the metal, so we refrain from separately discussing $\Delta E^{\ddagger}$ values. The most important trends in Table 5 are that activation enthalpies associated with **2**-H and **2**-Cl are about the same for a

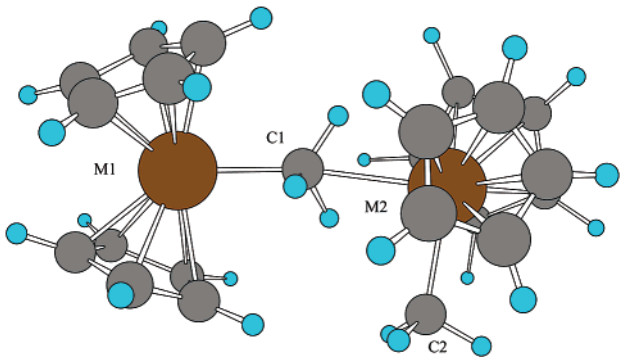

Figure 3. Optimized structure (B3LYP/ECP1) of $[(Cp)_2LuCH_3]_2$. See caption to Figure 1 for atom legend. Labeling is general for all dimers **4**.

Table 4. Selected Bond Distances (Å) and Bond Angles (deg) in 4 at the B3LYP/ECP1 Level[a]

	M		
	Sc	Y	Lu[b]
	Bond Lengths		
M1−C1	2.273	2.445	2.405 (2.437)
M2−C1	2.739	2.801	2.762 (2.760)
M2−C2	2.250	2.407	2.374 (2.357)
M1−M2	4.993	5.228	5.144 (5.177)
M1−Ω[c]	2.190	2.373	2.342 (2.30)
M2−Ω[c]	2.248	2.421	2.400 (2.37)
	Bond Angles		
M1−C1−M2	169.8	170.5	169.1 (170.0)
C1−M2−C2	87.1	89.3	88.7 (91.6)
Ω−M1−Ω	138.0	138.0	136.9 (139.0)
Ω−M2−Ω	132.6	132.1	131.0 (136.2)

[a] See Figure 3 for atom labeling in structure **4**; Ω refers to the centroid of a Cp ring bonded to the specific metal included in the degree of freedom. [b] Values in parentheses are from an X-ray crystal structure of $[(Cp^*)_2LuCH_3]_2$; metal centroid distances were reported to only two places after the decimal point. [c] Average of two distances.

Table 5. Methane Displacement TS and Dimer Energies and 298 K Enthalpies (kcal mol^{-1}) Relative to L_2MCH_3 Monomers at the B3LYP/ECP1 Level

		2		**3**		**4**	
L	M	$\Delta E^{\ddagger}$	$\Delta H^{\ddagger}_{298}$	$\Delta E^{\ddagger}$	$\Delta H^{\ddagger}_{298}$	ΔE	ΔH_{298}
H	Sc	15.3	13.8				
	Y	16.8	15.0				
	Lu	19.5	17.6			−17.3	−15.6
Cl	Sc	16.3	14.7				
	Y	17.0	15.2			−16.8	−15.3
	Lu	20.0	18.0				
Cp	Sc	22.8	21.6			−5.8	−4.6
	Y	20.8	18.6			−12.4	−11.3
	Lu	23.5	21.1	38.9[a]	35.8[a]	−12.2	−11.2
Cp*	Sc	26.8	25.7	33.0	30.8		
	Y	22.8	21.5	34.5	31.5		
	Lu	25.6	24.1	39.2	36.0		

[a] The Cp rings in this case are undecorated with methyl groups except for the one that is required for the reaction.

given metal, but these values are roughly 7 kcal mol^{-1} lower than the corresponding value for **2**-Cp,Sc, and 3 kcal mol^{-1} lower than the corresponding values for **2**-Cp,Y and **2**-Cp,Lu. Furthermore, the activation enthalpies computed for **2**-Cp are all 3−4 kcal mol^{-1} lower than the values computed for the corresponding compounds **2**-Cp*. This leads to rather substantial errors if, say, one attempts to infer the activation enthalpy associated with **2**-Cp*,Sc (25.7 kcal mol^{-1}) from **2**-H,Sc (13.8 kcal mol^{-1}).

The chemical basis for the computed trend is associated primarily with metal electrophilicity. The H-atom-transfer TS structure is stabilized by interaction of the occupied orbitals of the CH_3 - - H - - CH_3 fragment (in this case fully bonding and nonbonding σ-allyl-like orbitals) with appropriate metal d orbitals. The more electrophilic the metal, the lower the energy of the empty d orbitals and the more effective the stabilization of the TS structure (note that the intent is not to compare one metal to another, since issues of orbital overlap would then arise, but rather to compare electrophilicity of a given metal atom as a function of ligands). Ligands H and Cl are typically thought of as two-electron donors, and activation enthalpies are relatively insensitive to the change from one to the other. Cyclopentadienide rings, on the other hand, are formally six-electron donors and would be expected to significantly decrease overall metal electrophilicity; this is consistent with the higher activation enthalpies computed for Cp compared to H or Cl. Furthermore, methyl substitution on Cp makes Cp* an overall still stronger donor, and this is consistent with the incrementally higher activation enthalpies for the latter ligand. However, with Cp* it is also quite possible that steric effects may begin to play a significant role.

A secondary trend of considerable interest that speaks to that role is the reversal in relative *metal* reactivities that occurs with increasing ligand size. In the absence of any steric effects, i.e., with H or Cl ligands, the order of activation enthalpies is Sc < Y < Lu (presumably this trend derives at least in part from better overlap of the organic fragment orbitals noted above with d orbitals of lower quantum number). However, Watson and Parshall[2] have measured observed rate constants for methane exchange that show an activation enthalpy order of Y < Lu < Sc with Cp* (assuming no substantial difference in entropies of activation for any case). This same order of reactivity is predicted computationally for Cp or Cp* ligands, reflecting the greater steric congestion about Sc with its shorter bonds to these larger ligands.

To investigate further the quantitative utility of the calculations, we note that the ratio of rate constants reported by Watson and Parshall[2] for the **2**-Cp* series at 343 K is 5.7:1:0.022. We may use transition-state theory (rearranging eq 2 and again assuming an identical entropy of activation) to determine that this implies activation enthalpy differences of 1.2 kcal mol^{-1} between Y and Lu, 3.8 kcal mol^{-1} between Y and Sc, and 2.6 kcal mol^{-1} between Lu and Sc. The theoretical predictions in Table 5 for these comparisons are 2.6, 4.2, and 1.6 kcal mol^{-1}, respectively, which is an average error of 0.9 kcal mol^{-1}. Such agreement is quite encouraging. Note that with Cp in place of Cp*, these same comparisons are 2.5, 5.0, and 0.5 kcal mol^{-1}, respectively, which is an average error of 1.5 kcal mol^{-1}. Thus, replacing Cp* with Cp not only affects the absolute activation enthalpies by about 3 kcal mol^{-1} but also degrades the quality of the relative activation enthalpies.

For the lutetium case with Cp* ligands, Watson has carried out temperature-dependent rate constant measurements and reported an Eyring-plot-derived activation enthalpy. To compare this absolute activation enthalpy to a computed one, however, some account

needs to be taken of tunneling effects on the rate constant. We consider this comparison below, but delay for a moment to consider two other processes, namely, unimolecular methane ejection by formation of a tuck-in complex and metallocene dimerization.

Unimolecular Methane Displacement. On the basis of the bimolecular nature of the methane metathesis reaction rate (depending on both metallocene and methane concentrations), Watson and co-workers discarded the possibility that the metathesis mechanism involves a tuck-in complex. Nevertheless, it is interesting to examine the question of exactly how unfavorable that pathway is relative to the bimolecular one.

With full Cp* ligands, the enthalpies of activation associated with TS structures **3**-Cp* compared to **2**-Cp* are 5.1 kcal mol^{-1} higher for Sc, 10.0 kcal mol^{-1} higher for Y, and 11.9 kcal mol^{-1} higher for Lu. The smaller difference in the case of Sc is consistent with the shorter metal−ligand distances in this metallocene, thereby requiring less overall Cp* distortion to reach the TS structure.

From a purely enthalpic perspective, it is clear that the bimolecular process is favored over the unimolecular one in every instance, with the difference being quite substantial for Y and Lu. Of course, any analysis of rates for a unimolecular process compared to a bimolecular one must take into account the concentration of the reacting partner in the bimolecular process. Clearly at a sufficiently low methane concentration one would eventually find the unimolecular process to be kinetically dominant, although in that instance it would also be the case that the tuck-in complex would be the thermodynamic sink rather than simply an intermediate in a methane-exchange process. Indeed, in the Sc case, Thompson et al.[35] observed that prolonged heating of **1**-Cp*,Sc at 353 K led to methane production and a yellow, crystalline solid that, although it was not amenable to complete characterization, had a ^{1}H NMR spectrum consistent with it being the appropriate tuck-in complex.

A separate point worth noting with respect to the universus bimolecular processes is that, although we do not consider our computed entropies of activation to be quantitatively accurate owing to the presence of many, many low-frequency normal modes, and thus refrain from discussing them, nevertheless it is clear that the entropy of activation for the bimolecular process will be much more negative than that for the unimolecular one. Thus, modification of the reaction temperature could also potentially be used to tune between the two pathways, particularly in the case of Sc, where the difference in activation enthalpies is the smallest.

A final point of technical interest addresses the importance of the "spectator" methyl groups on the Cp* rings. In the case of Lu, we have examined the analogue of **3**-Cp*,Lu where only one (reacting) methyl group is present on the otherwise undecorated Cp rings. As already noted above, geometric differences between this reduced model and **3**-Cp*,Lu are observed to be quite small. Furthermore, the computed activation enthalpies differ by only 0.2 kcal mol^{-1}. At least for this reaction, then, full Cp* rings do not seem to be a requirement for quantitative accuracy.

Dimerization. Watson and co-workers have reported that **1**-Cp*,Lu exists in cyclohexane solution in equilibrium with its dimer **4**-Cp*,Lu and that the equilibrium at typical experimental temperatures favors dimer by about 4:1.[2,3,17] From a van't Hoff plot, they determined an enthalpy of dimerization of −12.6 kcal mol^{-1}.

From a computational standpoint, **4**-Cp*,Lu is technically challenging in size. We have, however, computed dimerization enthalpies for **4**-Cp (Table 5). For Sc, Y, and Lu, these values are −4.6, −11.3, and −11.2 kcal mol^{-1}, respectively. Again, the greater crowding of ligands about the smaller Sc atom leads to a qualitative difference between this metal and the other two. The comparison of the computed **4**-Cp,Lu value with the experimental one for **4**-Cp*,Lu is reasonably good, suggesting that the overall geometry is sufficiently structured to accommodate the 20 methyl groups in the permethylmetallocene. As already noted above, a direct comparison of the geometries of computed **4**-Cp,Lu and experimental **4**-Cp*,Lu also reveals them to be in good accord.

To assess further dimerization sensitivity to ligand effects, we computed the enthalpy of dimerization of **1**-H,Lu to form **4**-H,Lu. With the ligands reduced to hydride, the dimerization enthalpy becomes more favorable by 4.4 kcal mol^{-1}. The magnitude of this difference is about the same as that seen when comparing H to Cp for the activation enthalpies associated with **2** and **3**, suggesting that the electronic and steric differences between these ligands manifest themselves in similar ways in these disparate processes.

As a technical point, we note that all enthalpic comparisons made thus far have been between gas-phase theoretical models and experimental measurements made in cyclohexane solution. The good agreement we have observed up to this point suggests that neglecting to account for solvation effects associated with this very nonpolar solvent does not have a significantly adverse effect on such comparisons.

Tunneling Effects on the Reaction Coordinate. From an Eyring plot, Watson et al. determined the enthalpy and entropy of activation for methane exchange through TS structure **2**-Cp*,Lu to be 11.6 kcal mol^{-1} and −38.1 eu, respectively.[3] Although we have emphasized above the excellent performance of theory in predicting the relative activation enthalpies for Sc versus Y versus Lu, the absolute experimental value for **2**-Cp*,Lu is obviously substantially lower than the computed value of 24.1 kcal mol^{-1}. One possible reason for this difference might be associated with poor performance of the B3LYP/ECP1 model, despite its otherwise good accuracy when comparing geometries and dimerization. Single-point calculations with the *m*PWPW91/ECP2 model predict a somewhat reduced enthalpy of activation of 20.3 kcal mol^{-1}, but this is still in very poor agreement with the experimental value.

However, the reaction in question involves a substantial component of hydrogenic motion in the reaction coordinate, and as such it is quite possible that quantum mechanical tunneling contributes significantly to the overall reaction rate. Since tunneling becomes increasingly important at lower temperatures, Eyring plots over temperature ranges where tunneling does make significant contributions to the rate tend to predict

Table 6. Transmission Coefficients Predicted for Reaction through 2-Cp*,Lu and Observed and Classical Rate Constants at Different Temperatures[a]

T, K	$k_{obs} \times 10^5$, s^{-1}	κ	$k_{class} \times 10^5$, s^{-1}
300	10	93	0.11
330	67	24	2.8
340	120	13	8.8
350	200	9.2	21
360	320	7.2	45
370	510	5.9	87
380	800	5.0	160
390	1200	4.4	270
400	1800	4.0	460

[a] See eqs 1−5 in Computational Methods. All values to two significant figures.

enthalpies of activation that are lower than those associated with the zero-point-including potential-energy surface. As described in the Computational Methods section, we have assessed the degree to which tunneling influences the Eyring-plot-derived experimental enthalpy of activation by computing transmission coefficients κ via the Skodje−Truhlar method[67] for H transfer in TS structure **2**-Cp*,Lu at various temperatures within the range 300−400 K (Table 6; data for 310 and 320 K are not included because at these temperatures α and β are very nearly equal—their relative magnitudes invert at about 314 K—and this leads to some numerical instability in solving eq 3). At 300 K, tunneling is predicted to increase the rate of the reaction by just under 2 orders of magnitude, while at the top end of the range, 400 K, there is only a 4-fold rate acceleration.

If the tunneling contribution is removed from k_{obs} according to eq 1, the remaining k_{class} values may themselves be employed in an Eyring plot. Using the data in the right-hand column of Table 6 for such a plot results in a "corrected experimental" *semiclassical* enthalpy of activation of 19.2 kcal mol^{-1} ($R^2 = 0.994$); that is, the tunneling correction gives rise to a 7.6 kcal mol^{-1} change in the semiclassical activation enthalpy. This new value varies from the one derived from computation of the molecular partition function using the *m*PWPW91/ECP2 model by only 1.1 kcal mol^{-1}, an error of about the magnitude seen for other comparisons in this paper. It should be noted, moreover, that the Skodje−Truhlar method evaluates only the tunneling contribution along the reaction coordinate, i.e., through a single dimension of the multidimensional potential-energy surface. Accounting for multidimensional tunneling would be expected to increase κ still more, and thus would be likely to decrease the remaining error.

The importance of hydrogen atom tunneling even at temperatures above 300 K is an interesting observation. H/D kinetic isotope effects would be expected to be very large in this system, but no experimental measurement along these lines appears to have yet been made. From our calculations, we predict $k_H/k_D = 13.3$ at 340 K for the h_7 versus d_7 reactants (i.e., isotopic substitution of all methyl and methane positions).

Significance

The modeling of L_2MCH_3 species where L = H, Cl, Cp, and Cp* and M = Sc, Y, and Lu is accomplished efficiently at the B3LYP/ECP1 level, particularly with regard to molecular structures as judged by comparison to two X-ray crystal structures and other levels of theory. To accurately model the energetics of methane metathesis at the metal center requires that Cp* ligands be represented in full; simplification by use of Cp in place of Cp* reduces the enthalpy of activation by 3−4 kcal mol^{-1}, and use of model ligands H and Cl increases this error by still larger margins.

Comparison of the activation enthalpies for unimolecular methane ejection via formation of a tuck-in complex versus bimolecular methane metathesis indicates the former potentially to be a competitive process for Sc, but to be sufficiently higher in energy for Y and Lu to be unlikely to be thermodynamically significant under typical sets of reaction conditions. The greater propensity for Sc to form a tuck-in complex is related to the shorter metal−ligand distances observed for this metal atom.

Estimates of tunneling contributions to the overall rate of methane metathesis indicate that over the temperature range 300−400 K tunneling enhances the rate by factors of 4−93. When tunneling is accounted for in the experimentally observed rate constants, a semiclassical enthalpy of activation of 19.2 kcal mol^{-1} is determined for the methane metathesis reaction, which is in good agreement with the best theoretical prediction of 20.3 kcal mol^{-1}.

Acknowledgment. We thank Dr. J. C. Calabrese for providing us with the full X-ray crystal structure coordinates for **4**-Cp*,Lu.

Supporting Information Available: Cartesian coordinates for all optimized theoretical structures.

OM0209632